Tierney, M., Ketteringham, L., Selwyn, B., & Saidani-Scott, H. (2016). Calorimetric measurements of the dynamics of a finned adsorbent; early assessment of the activated 3 carbon cloth - ethanol pair with prismatic aluminium fins. Applied Thermal Engineering, 93, 1264-1272. DOI: 10.1016/j.applthermaleng.2015.10.009

Peer reviewed version

# Calorimetric measurements of the dynamics of a finned adsorbent; early assessment of the activated carbon cloth - ethanol pair with prismatic aluminium fins

M. Tierney[1], L. Ketteringham, R. Selwyn, H. Saidani

*1/ Corresponding author. Tel +44(0)117 3315903, e-mail mike.tierney@bristol.ac.uk*

## Abstract

The heat of adsorption of the pair ethanol-activated carbon cloth (ACC) has been measured in a specialised calorimeter, following a step change in vapour pressure (the "large pressure jump", LPJ) or a step change in temperature of the fin base (the “large temperature jump”, LTJ). This is the first time that LTJ has been attempted with this particular technique. The ACC was incorporated into a set of fins, representing small sections of finned tube adsorbent bed (~50 gram mass) and with a fin-to-fin gap of 6 mm. The heat rejection fitted an exponential decay, and for purposes of data fitting was adequately described by exponential decay, notwithstanding multiple physical effects within the ACC pack. Characteristic times, $\tau$, were established for LPJ and LTJ. The characteristic times were adjusted to allow for sensible heat of the sample, making them indicative of change in refrigerant uptake and cooling power. For instance, for the LTJ 338 K $\rightarrow$ 303 K the characteristic time was 146 s without adjustment, but 183 s with adjustment. For the fins tested under LTJ, an “average” specific cooling power, defined with cycle time = 1.6 $\tau$, was in the range of 0.36 to 0.52 kW kg$^{-1}$, somewhat smaller than seen elsewhere and requiring future optimization of the finned sample.

Keywords: AHP, calorimetry, activated carbon cloth

## Highlights

- A calorimeter housed sections of finned adsorbent.
- Both LTJ and LPJ tests were implemented.
- Exponential recovery fitted heat transfer adequately.
- Tentative estimates of SCP was made.

## Nomenclature

| | | |
|---|---|---|
| A | term related to adsorption potential | K |
| $A_{ACC}$ | External area of ACC | $m^2$ |
| $A_{fin}$ | External area of fins | $m^2$ |
| c | specific heat capacity of refrigerant | J/ (kg K) |
| $h_{ads}$ | specific heat of adsorption | J/ kg |
| $m_x$ | mass of adsorbent | kg |
| p | vapour pressure | Pa |
| $Q_a$ | heat accepted by sample, via fin base | J |
| SCP | specific cooling power | W/ kg (adsorbent) |
| t | time | s |
| $T_b$ | temperature measured at fin base | K |
| $T_v$ | temperature of refrigerant vapour | K |
| x | axial distance along fin | m |
| X | adsorbent loading | kg (adsorbate)/ kg (adsorbent) |
| $X^*$ | adsorption capacity (loading under equilibrium) | kg (adsorbate)/ kg (adsorbent) |

Greek Symbols

| | | |
|---|---|---|
| $\alpha$ | Heat transfer coefficient | W/ ($m^2$ K) |
| $\varepsilon$ | Thermal emissivity | - |
| $\kappa$ | Thermal diffusivity | $m^2$/ s |
| $\lambda$ | Thermal conductivity | W/ (m K) |
| $\sigma$ | Stefan-Boltzmann constant | W/ ($m^2$ $K^4$) |

Subscripts

| | |
|---|---|
| a | raw measurement of heat transfer |
| ads,etoh | property of ethanol in its adsorbed phase |
| al | property of aluminium |
| evap | evaporator condition |
| cond | condenser condition |
| f | liquid phase |
| g | vapour phase |
| i | refers to parts of sample (aluminium, activated carbon, adsorbate (ethanol) |
| lc | correction to heat loss based on steady state measurement |
| lm | calculated heat loss |
| mid | mid-point of fin |
| p,r | refrigerant vapour at constant pressure |
| sat | saturation temperature or pressure |
| x | sensible heat |
| w | vessel wall |

Superscripts

| | |
|---|---|
| (a-l) | raw heat transfer corrected for heat loss |

(a-lx) raw heat transfer corrected for heat loss and sensible heat storage

## 1. Introduction

This paper concerns a set of calorimetric tests used to predict the energy performance of adsorption heat pumps (AHPs). AHPs can amplify heat, produce a refrigeration effect from low grade heat (e.g. solar or waste heat), or both. It is worth noting the IEA's projection that solar heat could account for nearly 17% of energy use for cooling by 2050 [1]. In particular, AHPs are suited to relatively small scale operation (<10kW) where the difficulties manifest with absorption chillers are not resolved cheaply. (Such difficulties include the requirement for a distillation column in ammonia-water systems, or crystallisation and the cost of a solution pump in LiBr-water systems). At present AHPs are at the start of their product life cycle and show relatively low market penetration. Product growth demands improved cooling power at realistic capital cost and good thermodynamic efficiency. Before an investment in a prototype is approved it is useful to predict its likely performance. Our aim has been to develop a bench scale test appropriate to the most important part of the AHP's "thermal compressor" - the combinations of fins and adsorbent.

Packed beds or multiple layers of adsorbent generally exhibit low thermal conductivities, ~ 0.1 W $m^{-1}$ $K^{-1}$. This necessitates the use of extended heat transfer surfaces, or enhancement of the conductivity of the adsorbent, or both. Often adsorbent beads or fibres are located between fins [2]. Figure 1 shows the location of fin and adsorbent (items 2 and 3) and the associated thermal cycle (described in [3]). Alternatively, adsorbents can be coated to surfaces with a binder [4, 5] or grown onto substrates by hydrothermal synthesis [6], or adsorbent can be mixed with expanded graphite and compressed at high pressure to form a consolidated layer [3]. Whatever arrangement is chosen, the rate of adsorption is inevitably influenced by multiple factors. The thermal conductivity of the adsorbent is important, but so too is its vapour permeability - consolidation enhances conductivity at the expense of permeability. Contact resistances between grains of adsorbent or between grains and the heat transfer surface also play a role. The shape of the adsorption isobar is of interest. Other factors of the adsorbent

include thermal conductivity and pore diffusivity. It is laborious to acquire a large measurement set [7], and to incorporate it into a model of a complete system.

A simpler procedure is to measure refrigerant uptake under boundary conditions representing those in a working cycle - the "large temperature jump" (LTJ, for example Okunev et al [8]). In earlier developments of this technique, single grains resting on a metallic plate are subjected to near step changes in temperature. Rates of vapour uptake are inferred from small (~2 mbar) pressure changes in an isothermal vessel, typically one would expect about 20-litres in volume (for water vapour and a 40 mg grain). LTJ contrasts with tests employing a "large pressure jump", or LPJ [9]. LTJ was applied to sample sizes of 0.314 g (Silica Fujii RD), stacked in monolayer or multiple layers [10], to investigate the impact of number of layers, grain size, and the important ratio S/m (S is contact surface area, m is dry sample mass). Adsorption loading was generally fitted to an exponential recovery, although a "tail of the kinetic curve can be slower than exponential" particularly for smaller grains stacked in thicker layers. This variant of LTJ is sometimes termed "constant volume variable pressure" or "V-LTJ" (V = volumetric) but more recently G-LTJ (G = gravimetric) has allowed real time weighing of up to 600 g of heat exchanger plus sample to accuracy of 0.1 g [11]. A first set of experiments considered single and multiple layers of sorbent (commercial SAPO-34 adsorbent). "Hydrodynamic forces", from the cooling/ heating system, disturbed weight measurement (apparently about ± 1.5 g max. according to their Fig. 6) but the authors imply that this noise can be filtered in a satisfactorily way. The characteristic time for change in plate temperature was 25 s, and measured adsorption loadings were fitted to an exponential recovery. A subsequent paper [12] tackled pieces of real adsorbers, based on a commercial flat-tube HEX, 360 louvred fins/ metre packed with 73 g to 90 g AQSOA. As in [10] desorption rates were 1.5 times faster than adsorption rates, possibly owing to higher average temperature and pressure. The AdHex was 1.5 to 2.0 times slower than the 'ideal' flat plate configuration. (Similarly [10] claimed a factor of difference 2 to 6 between their LTJ and "real" AHPs).

Rather than passing coolant through a test vessel, or using a very large reservoir, Ahamat and Tierney [13] employed a thermoelectric method wherein 5 g of silica gel was bonded to aluminium. The location of their heat source/ sink (a thermoelectric module) outside the test-vessel rendered the experiment appropriate for minimal variation in indicated temperature, viz the LPJ. The direct measurement of heat (or mass in the case of [11]) obviated the need for a very large vapour reservoir. The heat addition to the evaporator was also measured. (Van Heyden et al [14] show one illustrative result with a heat flux meter, under LPJ.)

The work reported here was motivated by the construction of an AHP prototype at the University of Bristol, broadly comprising the components listed in Figure 1. The thermoelectric method was adapted for a combination of fins and adsorbent, termed "Ad-HEX". The fin-to-fin gap was the same as that in the prototype chiller [15], and ethanol-activated carbon was chosen as the active pair in conformity with the prototype, and it is intended that ultimately results from these experiments could be used to predict the prototype performance. Rates of heat rejection from the fin base were measured under both LPJ and LTJ. Characteristic times are reported as (a) the direct heat transfer from the fin base to the TEM, relating to the net thermal power input to an Ad-Hex, and (b) the aforementioned heat transfer corrected for changes in sensible energy, relating to the cooling power of an evaporator. For LPJ the adjustment had minimal impact for the net heat transferred between start and end of the experiment (because the two states shared the same temperature). This permitted the inference of adsorption capacities for comparison with gravimetrically measurements – the same check was used in [13]. For both LPJ and LTJ direct and adjusted rates of heat transfer were close to exponential decay. In discussion, characteristic times are employed to offer tentative estimates of specific cooling power (SCP).

## 2. Methods and Procedure

The methods comprised measurement of the heat rejected by adsorption in real time, gravimetric checks of adsorption capacity, and incorporation of these data into an estimate of specific cooling power.

Fig. 2 shows the calorimeter, housed in a vapour vessel. Pressures were measured with an Edwards active strain gauge (model D 35726000) and the vessel could be connected to an evaporator (via V1) or a vacuum pump (via V2). The vessel contained an instrumented sample bonded to a thermo-electric module (TEM, GCS model ET-161-12-10-E).

The TEM was calibrated to sense heat flows; we subjected a cubiform aluminium block to cooling curves, following procedures in [16]. The newer GCS module employed a more rugged solder and thus allowed operation at temperatures up 373 K, rather than the previous upper limit of 353 K in reference [13]. The heat input (or output) was estimated from three principal effects: the Peltier effect proper, ohmic heating, and thermal conduction between the two faces of the module. The calculation inputs comprised electric properties of the TEM, measured potential difference, electrical current, and face temperature. A sensitivity analysis indicated measurement uncertainties of ±10%, confirmed by the inference of adsorption capacities to within 10% of gravimetric data [13]. To eliminate some stray heat losses, the TEM in the present work was located inside the vapour vessel rather than outside. It was bonded to a sample of finning with matching face area.

Each sample comprised a set of aluminium fins with layers of Chemviron FM50 ACC sandwiched within each fin-to-fin gap. Fig. 3 shows the sample used with LPJ conditions. Ethanol was the adsorptive. (Aristov [17] includes its adsorption on various microporous carbons (similarly methanol, carbon dioxide, and ammonia) in his analysis of an adsorbent database. He notes that preferred equilibrium equations follow from Polyanyi potential theory, and in particular the Dubinin-Radushkevich equation). Table 1 lists the fin dimensions. The lighter set of fins was fabricated so as to enable the large temperature jump. The fins and their base were wire cut from the same aluminium block to eliminate thermal resistances between base and fin root. The base was coated with thermal paste (Shinetsu-

X2307762-S) and laid onto the TEM; the TEM was similarly coated and laid onto the lid of the vapour vessel. A K-type thermocouple was secured to the fin base for purposes of temperature control; a second thermocouple was located inside the ACC layer. Four 1.5-mm diameter nylon screws secured the assembly to the lid of the vapour vessel. Prior to insertion in the calorimeter, the sample had been held at 393 K for six hours to desorb impurities. It was transferred to the vapour vessel quickly then heated to 373 K (by the TEM) under vacuum, for four hours. The sample was then brought to its set-point temperature in readiness for experiments.

**Table 1 Sample dimensions. A lighter sample was used for large temperature jump experiments. Eight layers of ACC were sandwiched between each fin-to-fin gap**

| Dimension | Large pressure jump | Large temperature jump |
|---|---|---|
| Area of base | 40 mm x 40 mm | 40 mm x 40 mm |
| Thickness of base | 3 mm | 1.5 mm |
| Fin length | 40 mm | 40 mm |
| Number of fins | 6 | 7 |
| Fin-to-fin distance | 6 mm | 6 mm |
| Thickness of fin | 1.5 mm | 0.4 mm |
| Mass of aluminium part | 50.4 g | 19.2 g |
| Mass of ACC (dry) | 14.0 g | 14.0 g |

Samples were subjected to two types of boundary conditions. For a "large pressure jump" (LPJ, [9]) the evacuated vapour vessel and evaporator were initially unconnected (V1 closed) and each brought independently to steady state at specified temperatures. The experiment was started by means of opening the connecting valve (V1 on Fig. 2) after which the current to the TEM was controlled to maintain constant the measured temperature at the base of the fins. For a "large temperature jump" (LTJ, [18]) the connecting valve V1 was open throughout the experiment. Initially the complete system was allowed to reach equilibrium. The experiment started with a fast reduction in set point; the nominal (base) temperature required about 12 s to achieve its new set point.

## 3. Analysis of Data

Consider the experiment at an initial equilibrium state, suddenly perturbed at time t = 0 (either by LPJ or LTJ) so that by time (t) a net amount of heat $Q_a$ (in joules) must be added to the fin base. Heat $Q_a$ was corrected for (1) estimated heat losses plus a minor calibration offset, giving $Q^{(a-l)}$ (2) further, the sensible heat storage in the aluminium structure, ACC and sorbate, giving $Q^{(a-lx)}$ and relating to mass of vapour adsorbed and adsorption loading X. The corrections necessitated the computation of average ACC temperature and average fin temperature; the temperatures at the fin base and in the ACC formed required boundary conditions (location 5 in Fig. 2). In the results section $Q^{(a-l)}$ and $Q^{(a-lx)}$ and are fitted to exponential decay; the characteristic times enable estimates of cooling power. They are defined as,

$$Q^{(a-l)}(t) = Q_a(t) - Q_{lm}(t) - Q_{lc}(t) \quad [1]$$

$$Q^{(a-lx)}(t) = Q_a(t) - Q_{lm}(t) - Q_{lc}(t) - \sum Q_{x,i}(t) \quad [2]$$

where $Q_{lm}$ is an estimated heat loss, minor correction $Q_{lc}$ ensures $dQ^{(a-l)}/dt = 0$ under measured steady conditions, and $Q_{x,i}$ allows for sensible heat storage. Also subscript i refers to sample parts (i = aluminium, activated carbon, adsorbate (ethanol)). Convective and radiative losses were computed.

$$\frac{dQ_{lm}}{dt} \approx A_{fin}\left(\varepsilon_{al}\,\sigma\left(T_{fin,av}^4 - T_w^4\right) + \alpha\left(T_{fin,av} - T_w\right)\right) \quad [3]$$

$$+ \quad A_{ACC}\left(\varepsilon_{ACC}\,\sigma\left(T_{acc,av}^4 - T_w^4\right) + \alpha\left(T_{acc,av} - T_w\right)\right)$$

where the aluminium part of the sample has exterior surface area $A_{fin}$ and emissivity $\varepsilon_{al} = 0.095$ [19] and the ACC part has exterior surface area $A_{ACC}$ and emissivity $\varepsilon_{ACC} = 0.85$ [20]. Also $T_w$ is the temperature of the vessel wall, $\sigma$ is the Stefan-Boltzmann constant, and $\alpha$ is a heat transfer for natural convection, e.g. for the four vertical sides [21] is recommended for laminar natural convection. Inevitably small mismatches (~0.3 W) existed between computed heat loss, and measured loss $Q_a$ under steady conditions at start ($t \leq 0$) and end ($t \to \infty$) of experiment, partly owing to uncertainty in correlations and partly owing

to any nonlinearity in TEM properties. The steady state correction was defined as $Q_{lc} = Q_a - Q_{lm}$, so that more generally

$$\frac{dQ_{lc}(t)}{dt} = \frac{dQ_{lc,start}}{dt} + \left(\frac{dQ_{lc,end}}{dt} - \frac{dQ_{lc,start}}{dt}\right) \frac{T_b(t) - T_{b,start}}{T_{b,end} - T_{b,start}} \quad [3]$$

where "start" indicates $t \leq 0$ and "end" indicates $t \to \infty$. For simplicity, this small correction was varied according to temperature of the fin base.

Estimates of sensible heat employed the initial temperature of the fin base as a datum

$$Q_{x,i}(t) \approx m_i c_{pi} \left(T_{i,av}(t) - T_b(0)\right) \quad [5]$$

To obtain the temperature profile along the fin (and hence the average temperature of the fin) the general conduction equation [22] was reduced to one dimension (line A-A in Figure 2).

$$\frac{1}{\kappa}\frac{\partial T}{\partial t} = \frac{\partial^2 T}{\partial x^2} + \frac{1}{\lambda V_{fin}} \frac{\partial Q_{fin}}{\partial t} \quad [6]$$

where $V_{fin}$ is the fin volume, x is displacement along AA, $\kappa$ is thermal diffusivity (of aluminium), and $\lambda$ is thermal conductivity. The boundary coefficients were a Dirichlet condition at the base of the fin ($T = T_b$ at x=0) and adiabatic fin tip ($dT/dx = 0$). Term $Q_{fin}$ is the heat transferred to the flanks of the fins, approximated as $\delta Q_{fin} \approx \delta Q^{(a\text{-}lx)}$ with $\delta Q^{(a\text{-}lx)}$ taken from the previous recorded time. The numerical solution comprised the explicit forward difference method. Numerical integration of the temperate profile (along AA) yielded average temperature, $T_{fin,av}$.

Initially, the profile in the activated carbon (line BB in Fig. 2) was also attacked with the general conduction equation [22], choosing a thermal conductivity that gave best fit to measured ACC temperature, but this method exhibited unacceptable overshoots in prediction. Instead

$$T_{acc,av} \approx w T_{fin,mid} + (1 - w)\, T_{ACC,mid} \quad [7]$$

where weighting w = 1/3 corresponds to quasi-equilibrium solution of the general conduction equation ( $\partial T/\partial t \rightarrow 0$) along line BB, Fig. 2. Term $T_{ACC,mid}$ is the measured temperature of ACC (point 5, Fig. 2). The profile takes parabolic form (page 512 in [22]) with coefficients deduced from the known end temperatures ($T_{fin,mid}$ and $T_{ACC,mid}$) and the zero temperature gradient at the centre of line BB. On integration w = 1/3 in Equation 7.

Whereas the principle measurement was heat transfer, $Q_a$, elsewhere it tends to be adsorption loading, X. A heat balance gives,

$$X(t) \approx \frac{-Q^{(a-lx)}}{m_x\left(h_{ads} - c_{p,r}\left(T_{ACC,av}(t) - T_v\right)\right)} + X(0) \qquad [8]$$

where $c_{p,r}$ is the specific heat of the refrigerant vapour at constant pressure. With regard to LPJ, initially the ACC is dry and X(0) = 0. Very close sample temperatures at start and end mean that all $Q_x(\infty) \rightarrow 0$ and adsorption capacity $X^* = X(t \rightarrow \infty)$ is in direct proportion to $Q^{(a-l)}$, permitting comparison of gravimetric and calorimetric measurements. More generally, loading X(t) has been observed elsewhere to follow a near exponential recovery, both for LPJ and LTJ. If the denominator in Equation [8] is approximately constant the same can be expected for corrected heat flows. To facilitate later discussion two characteristic times were found by means of MATLAB's curve fitting tool (cftool).

*Full correction of raw data (a-lx)*

$$Q^{(a-lx)} = Q_o^{(a-lx)}(1 - \exp(-t / \tau_{a-lx})) \qquad [9]$$

*Correction for heat loss only (a-l)*

$$Q^{(a-l)} = Q_o^{(a-l)}(1 - \exp(-t / \tau_{a-l})) \qquad [10]$$

Very tentative estimates of chiller performance were made, neglecting in particular the heat capacity of any casing connected to the Ad-HEX. In [11] the exponential recovery of X(t) versus time

(in LTJ) was manipulated to yield specific cooling power. In a similar approach, Equation 11 yields the cycle averaged cooling power as a function of cycle time,

$$SCP_{avg} = \frac{Q_o^{(a-lx)}}{m_x\, t_{cycle}}\left(1 - \exp\left(-t_{cycle} / \tau_{a-lx}\right)\right)\frac{\left(h_{fg} - c_{p,r}\left(T_{cond} - T_{evap}\right)\right)}{\left(h_{ads} - c_{p,r}\left(T_{ACC,av} - T_{evap}\right)\right)} \qquad [11]$$

It has been suggested to stop an isobaric stage when uptake reaches 70%-to-90% [11] and indeed $SCP_{avg}$ is half its maximum value at 80% uptake (and here $t_{cycle} = 1.6\ \tau_{a-lx}$).

## 4. Results

Samples were subjected to LPJs, to provide recordings of heat rejection for comparison against gravimetric assessment (via Equation 8, one notes $Q^{(a-lx)} \rightarrow Q^{(a-l)}$ as $t \rightarrow \infty$). Kinetic data were ascertained for a LTJ – in the discussion section the broad implications for chiller performance are discussed. The final paragraph in this section analyses experimental error.

The LPJ was arranged with set points in the range from 303 K to 358 K. Refrigerant was rapidly introduced to the test section, usually at a pressure of 19 mbar ($T_{sat}$ = 275 K). Fig. 4 shows heat rejection from the fin base (~ 2 watts) before the start of the pressure jump; the previous section describes correction. During the LPJ base temperatures remained nearly constant, but in the centre of the layers of ACC temperature spikes measured up to 30 K (Fig. 5). All temperatures eventually regained their initial values so that between the start and end of each experiment the sensible energy of the sample had changed minimally. Corrected heat rejection was recorded against time for a range of fin base temperatures and each curve fitted an exponential decay; $r^2 > 98\%$ (Fig. 6). Table 2 presents the two sets of characteristic times defined in Equations 9 and 10. Note (Fig. 5) cooling of the fin base but an initial temperature rise in the ACC so that fitting gives $\tau_{a-lx} < \tau_{a-l}$. The adsorption capacity ($X^*$) was inferred from the final heat rejection (Equation [8] taking Q at $t \rightarrow \infty$). To obtain a check on adsorption capacity the test section was disassembled and the fin-plus-ACC weighed. The comparison is fair (Fig. 7);

adsorption capacities were fitted to the Dubinin-Radushkevich (DR) equation in conformity with other workers [23]. (The quality of data, $r^2$ = 92.75%, did not encourage detailed comparison of isotherm types.)

**Table 2 Time constants for LPJ**

| Base temperature $T_b$, K | Full correction (Eqn. 7) | | | Correct stray heat loss only (Eqn. 8) | | |
|---|---|---|---|---|---|---|
| | $Q_o^{(a-lx)}$, J | $\tau_{a-lx}$ , s | $r^2$ | $Q_o^{(a-l)}$ | $\tau_{a-l}$ , s | $r^2$ |
| 303 | -3575 | 318 | 0.98 | -3743 | 400 | 0.99 |
| 313 | -2501 | 226 | 0.98 | -2588 | 286 | 0.99 |
| 323 | -2106 | 200 | 0.98 | -2170 | 238 | 0.99 |
| 333 | -1324 | 177 | 0.97 | -1332 | 162 | 0.98 |
| 358 | -841 | 110 | 0.97 | -863 | 141 | 0.98 |

*Note that pressures were in the range 17 to 19 mbar.*

Fig. 8 shows the outcome of a large temperature jump, from 65°C to 30°C. Part (a) shows components of heat transfer – the total heat transfer (corrected for stray losses), $Q^{(a-l)}$, the estimated losses, $Q_{lm} + Q_{lc}$, the sensible heat $Q_x$ and its components. The second part shows the base temperature, the measured temperature in the centre of the ACC and predicted temperatures for the fin tip. One notes rapid reduction in fin base temperature, $T_b$, but a slower reduction in rate of heat transfer $Q^{(a-l)}$. Figure 9 shows the data fitting to heat transfer corrected for heat loss $Q^{(a-l)}$ and fully corrected $Q^{(a-lx)}$. Table 3 gives fitting parameters - $\tau$ and $Q_o$. Note (Figure 8) cooling of the fin base and a temperature fall in the ACC so that fitting gives $\tau_{a-lx} > \tau_{a-l}$. For purposes of comparison, $Q_o^{(a-lx)}$ is tabulated next to expected heat of adsorption, $m_x h_{ads} \Delta X^*$. For the four adsorption tests, both sets conform moderately well, but no so for the final desorption test. For this reason the desorption test is rejected from further discussion. (Generally desorption experiments demanded a larger heat supply and the net heat input tended to oscillate substantially – the control system requires upgrading.) Other than the desorption test, the characteristic times were restricted to narrow ranges, $\tau_{a-lx} \in$ [159s, 191s] and $\tau_{a-l} \in$ [127s, 154s] .

**Table 3 Time constants for LTJ**

| Base temp. $T_b$, K | Pressure, mbar | Correction for stray losses and sensible heat (a-lx) | | | | Correction for stray losses only (a-l) | | |
|---|---|---|---|---|---|---|---|---|
| | | $Q_o^{a\text{-}lx}$, J | $m_x h_{ads} \Delta X^*$ | $\tau_{a\text{-}lx}$, s | $r^2$ | $Q_o^{a\text{-}l}$ | $\tau_{a\text{-}l}$, s | $r^2$ |
| 338→303 | 22 to 27 | -2264 | -2167 | 183 | 0.9974 | -3351 | 146 | 0.9910 |
| 338→303 | 13 to 16 | -2403 | -2480 | 185 | 0.9994 | -3499 | 150 | 0.9940 |
| 360→303 | 20 to 24 | -3554 | -3654 | 191 | 0.9961 | -5337 | 154 | 0.9983 |
| 358→323 | 21 to 23 | -2308 | -2000 | 159 | 0.9860 | -3439 | 127 | 0.9695 |
| 303→338 | 20 to 23 | 1719 | 2190 | 325 | .9914 | 2737 | 192 | 0.9791 |

Estimated uncertainties in heat flow, temperature and pressure are summarised in Table 4.

**Table 4 Measurement uncertainties and error analysis**

| Item no | Source of uncertainty | Justification | Error |
|---|---|---|---|
| *Heat flow measurement* | | | |
| 1 | Measured heat flow | Assessed in [16] | 10.0% |
| 2 | Correction for extraneous heat loss | Prior to experiment, minimal variation from constant heat flow. Use higher estimate of ± 40 J from [13] | 1.6% |
| 3 | Refrigerant temperature in sample section is an estimate | In Equation [1], change estimate of $T_v$ from evaporator to vessel wall temperature | 3.8% |
| | **Total uncertainty** | $\sqrt{10^2 + 1.6^2 + 3.8^2}$ | 10.8% |
| *Temperature measurement* | | | |
| 4 | Sensor error | Thermocouple random error | 0.5 K |

## 5. Discussion

The relationship of characteristic time to underlying mechanisms is discussed. We estimate and tabulate the sensitivity of driving forces to temperature gradients in the fin-adsorbent system. A very tentative estimate of specific cooling power is made, on the basis of Equation 11.

277 Potentially, several mechanisms might have influenced adsorption kinetics. Temperature spikes in
278 the centre of the ACC, or temperatures that change far more slowly than the base temperature, indicate
279 the importance of thermal conduction. Temperature spikes in the centre of the ACC would have reduced
280 local adsorption capacities. (For example, a 30K spike in temperature would have reduced adsorption
281 capacity from 23% to 15% for conditions on Fig. 5.) Given the sophisticated interactions between many
282 physical processes, it is noteworthy that a simple near exponential relation between loading and time (and
283 here adjusted heat rejection and time) has been seen numerous times for many adsorbents and adsorbates
284 of different configurations.

285 The observed exponential functions do not have a strong theoretical basis. Exponential decay/
286 recovery has been observed in [8, 9, 13, 18, 24] with adsorbents on a flat, isothermal surface rather than
287 between fins, and then more recently in finned systems [12]. Approximately linear kinetics in grains were
288 first proposed by Gluekauf [25] (e.g. for spheres $dX/dt = 60\ (D_p/a_p^2)(X^*-X)$ where $a_p$ is characteristic
289 grain size and $D_p$ is intra-grain diffusivity). However, even for isothermal conditions the approach is
290 criticized for not faithfully reproducing Fickian Diffusion [26]. Nonetheless, some workers have
291 employed linear driving force models (LDF) to simulate adsorption heat pumps (e.g. [27], [28]) but more
292 recently LTJ has been proposed as giving a direct scaling to give the cooling power of real chillers with
293 no requirement for sophisticated modelling [10]. A benefit of using LTJ for finned structures is that in
294 mimicking AHP boundary conditions it accounts for the heat capacity of ACC and aluminium. A future
295 challenge for LTJ, particularly for smaller AHPs, might lie in allowing for steady and dynamic losses
296 through parts attached to the AHP such as its casing.

297 Calculated temperature gradients along the fins merit discussion. Estimates were made by solving
298 Equation 6. The first two rows in Table 5 shows the peak temperature differences from fin root to fin tip
299 (LPJ and LTJ). (For purposes of sensitivity analysis and for LTJ, measured base temperatures ($T_b$) were
300 replaced with an idealised step function). The table also shows corresponding reductions in adsorption
301 capacity, computed from the DR equation. Table 6 shows the temperature differences versus time. The
302 temperature differences were more important for the LTJ, partly owing to the nature of this boundary

condition and partly to a reduced fin thickness (0.4 mm rather than 1.5 mm). Higher local temperatures reduced the local driving force for adsorption.

The third row in Table 5 refers to the measured peak difference in temperature between ACC (mid-plane) and base; a corresponding (local) reduction in X* from 23% to 15% was computed.

In the fourth row in Table 5 we consider the permeability of the ACC (approximately $7x10^{-11}$ $m^2$, inferred from manufacturer's data). For an idealised one dimensional flow the calculated peak pressure difference from sample face to sample centre was 1.4 mbar with minimal impact on adsorption capacity.

Whereas the woven ACC offered good permeability, the processing of the fibres influenced adsorption capacity. The BET surface area was less than for the carbon fibres type A-15 and A-20 reported by El-Sharkawy et al [23] and in consequence the maximum adsorption capacity was reduced. (BET surface areas were 1900 $m^2$ $g^{-1}$ for A-20, 1400 $m^2$ $g^{-1}$ for A-15 and 1000 $m^2$ $g^{-1}$ for FM50K. The corresponding values of $X_o$ were 0.797, 0.570 and 0.398 kg (adsorbate)/ kg (adsorbent) respectively. )

No desorption tests are considered here (other than discounting the results of a single measurement). Previous evidence (for silica-gel-water) indicates (a) a back pressure was evident when the function of the evaporator was reversed and it acted as a condenser (b) under LPJ and for the same set point temperature, no measureable impact on kinetic constant (=1/τ), within error bands[29].

Sapienza et al [11] quote $SCP_{avg,80}$ = 0.56 kW $kg^{-1}$ for the LTJ (338K → 303 K) with SAPO24 monolayers of 2.4 mm to 2.6 mm diameter. (Here $t_{cycle}$ = 1.6 τ, after which the average SCP is 50% of its initial, maximum value and 80% change in uptake is achieved.) Equation 11 yields a comparable but lower value of 0.36 kW $kg^{-1}$ for the same temperature jump. More generally, our $SCP_{avg,80}$ are in the range 0.36 to 0.52 kW $kg^{-1}$. Sapienza investigates a range of grain sizes, as low as the range 0.350 mm to 0.425 mm at which far higher $SCP_{avg,80}$ = 4.4 kW $kg^{-1}$, although (a) for such small monolayers a high mass ratio (metal:adsorbent) will inevitably reduce coefficient of performance (b) when grains are stacked in multiple layers, so that the grain mass per unit surface area is a constant, there is a regime for which

328 $SCP_{avg,80}$ is independent of grain size. To boost $SCP_{avg,80}$ our future work requires thorough screening of
329 adsorbents, their BET surface area, and fin configurations (e.g. louvred fins, which would be filled with
330 granules rather than cloth). Although the choice of ACC-ethanol may not appear competitive here some
331 advantages for practical machines include (a) evaporation below the freezing point of water (b) for a
332 given evaporator temperature, a higher saturation pressure so that any ingress of air or other inert species
333 is mitigated (c) easier handling, cutting, and positioning of the adsorbent during manufacture.

334 **Table 5 Sensitivity Analysis**

335

| Effect | Consequence | $X^*$ reduced from 23% to … | Justification |
|---|---|---|---|
| Temperature gradients along fins during LPJ | Fin tip hotter than root. Local reduction in adsorption capacity | 21% at t = 40 s ($T_{tip}$-$T_{root}$ = 3.3 K) | DR equation Finite Difference See Table 6 |
| Temperature gradients along fins during LTJ | As above | 17% at t = 40 s ($T_{tip}$ - $T_{root}$ = 13 K) | DR equation Finite Difference See Table 6 |
| Temperature spikes in bulk of ACC (measured, LPJ) | Local reduction in adsorption capacity. $X^*$ | 15% at t = 40 s ($T_{mid}$-$T_{root}$ = 30K) | DR equation Measurement |
| Pressure loss through ACC | Lower $X^*$ in centre of ACC | 22.3% ($p - p_{mid}$ = 1.4 mbar) | DR Equation Manufacturer's permeability |

336
337 Pressure = 19 mbar and base temperature 323 K for estimates.

338

**Table 6 Predicted temperature difference from fin root to fin tip**

| time, s | 0 | 20 | 40 | 60 | 80 | 100 | 120 |
|---|---|---|---|---|---|---|---|
| LPJ, T = 323 K, p = 0→19 mbar | 0.0 | 3.2 | 3.3 | 3.1 | 2.9 | 2.6 | 2.4 |
| LTJ, T = 358 K→ 323 K, p = 19 mbar | 0.0 | 7.1 | 13.0 | 11.7 | 10.8 | 9.9 | 9.1 |

| time, s | 120 | 240 | 360 | 480 | 600 |
|---|---|---|---|---|---|
| LPJ, T = 323 K, p = 0→19 mbar | 2.4 | 1.5 | 0.9 | 0.6 | 0.3 |
| LTJ, T = 358 K→323 K, p = 19 mbar | 9.1 | 5.6 | 3.4 | 2.1 | 1.3 |

Pressure = 19 mbar and base temperature 323 K for estimates

## 6. Conclusions

The calorimetric test reported here is relatively new, and to date has been used in a limited number of tests for silica-gel water only. It offers a means of tackling relatively large samples of adsorbent – alongside gravimetric methods recently developed in [11, 12]. The test is extended to a different , adsorbent-adsorptive pair, and tackles finned samples. Also, mounting the thermoelectric module inside the test vessel has permitted the use of a large temperature jump (which recently has been applied elsewhere to pieces of AdHex). Our test dealt with samples representing sections of finned adsorbent. Notwithstanding numerous effects within the layers of ACC, the plot of heat rejection (from the fins' base) versus time took a near exponential form. Thereupon, characteristic times were deduced for tests with a step change in pressure (LPJ); these appeared to reduce with increased sample base temperature, $T_b$. Characteristic times were defined with and without correction for the heat capacity of the sample – the first relates more closely to changes in uptake and hence cooling power. The low estimated cooling power ($SCP_{avg,80}$ = 0.36 to 0.52 kW $kg^{-1}$) necessitates future optimization of fin configuration.

## Acknowledgements

The authors acknowledge funding from the Leverhulme Trust under grant reference F00182CD. The measurements of undergraduate students under the guidance of the authors is acknowledged, in particular A. Martin, B. Richards, and B. Turtle.

## References

1 https://www.iea.org/publications/freepublications/publication/technology-roadmap-solar-heating-and-cooling.html last viewed 25 September 2015

2 A.Rezk, R. K. Al-Dadah, S. Mahmoud, A. Elsayed, Effects of contact resistance and metal additives in finned-tube adsorbent beds on the performance of silica gel/water adsorption chiller, Applied Thermal Engineering 53(2) (2013) 278-284.

3 S. G.Wang, R. Z. Wang, X. R. Li, Research and development of consolidated adsorbent for adsorption systems, Renewable Energy 30(9) (2005) 1425-1441.

4 G.Restuccia, A. Freni, G. Maggio, A zeolite-coated bed for air conditioning adsorption systems: parametric study of heat and mass transfer by dynamic simulation, Applied Thermal Engineering 22(6) (2002) 619-630.

5 S. D. Waszkiewicz, M. J. Tierney, H. Saidani Scott, Development of coated, annular fins for adsorption chillers. Applied Thermal Engineering 29(11) (2009) 2222-2227.

6 L. Bonaccorsi, A. Freni, E. Proverbio, G. Restuccia, F.Russo, Zeolite coated copper foams for heat pumping applications. Microporous and Mesoporous Materials 91(1) (2006) 7-14.

7 L. W. Wang, Z.Tamainot-Telto, R.Thorpe, R. E. Critoph, S. J. Metcalf, R. Z. Wang, Study of thermal conductivity, permeability, and adsorption performance of consolidated composite activated carbon adsorbent for refrigeration, Renewable energy 36(8) (2011) 2062-2066.

8 B. N. Okunev, A. P. Gromov, L. I. Heifets, Y. I. Aristov, A new methodology of studying the dynamics of water sorption/desorption under real operating conditions of adsorption heat pumps: Modelling of coupled heat and mass transfer in a single adsorbent grain, Int. J. Heat Mass Transfer 51(1) (2008), 246-252.

9 B. N.Okunev, A. P.Gromov, L. I., Heifets, Y. I. Aristov, Dynamics of water sorption on a single adsorbent grain caused by a large pressure jump: Modeling of coupled heat and mass transfer, Int. J. Heat Mass Transfer 51(25) (2008) 5872-5876.

10 Y. I Aristov, I. S. Glaznev, I. S. Girnik, Optimization of adsorption dynamics in adsorptive chillers: Loose grains configuration, Energy 46 (1) (2012) 484-492.

11 Sapienza, S. Santamaria, A. Frazzica, A. Freni, Y. I. Aristov, Dynamic study of adsorbers by new gravimetric version of the Large Temperature Jump Method, Applied Energy 113 (2014) 1244-1251.

12 S. Santamaria, A. Sapienza, A. Frazzica, A. Freni. I. Girnik, Y.I. Aristov,Water adsorptive dynamics on representative pieces of real absorbers for adsorptive chillers, Applied Energy 134 (2014) 11-19.

13 M. A. Ahamat, M. J. Tierney, Calorimetric assessment of adsorbents bonded to metal surfaces: Application to type A silica gel bonded to aluminium. Applied Thermal Engineering, 40(3) (2012), 258-266.

14 H. van Heyden, G. Munz, L. Schnabel, F. Schmidt, S. Mintova, T. Bein, Kinetics of water adsorption in microporous aluminophosphate layers for regenerative heat exchangers, Applied Thermal Engineering 29(8) (2009) 1514-1522.
15 L. P. Ketteringham, M. J. Tierney, M. A. Ahamat, H. Saidani-Scott, R. Selwyn, Design and construction of a low cost solar chiller, with calorimetric assessment of the adsorbent bed. Presented at World Renewable Energy Forum (vol 2012) (2012).
16 M. A. Ahamat, M. J. Tierney, Timewise temperature control with heat metering using a thermoelectric module, Applied Thermal Engineering 31(8) (2011) 1421-1426.
17 Y. I. Aristov, Adsorptive transformation of heat: Principles of construction of adsorbents database, Applied Thermal Engineering 42 (2012) 18-24.
18 Y. I. Aristov, B. Dawoud, I. S. Glaznev, A. Elyas, A new methodology of studying the dynamics of water sorption/desorption under real operating conditions of adsorption heat pumps: experiment, Int. J. Heat Mass Transfer 51(19) (2008) 4966-4972.
19 J. R. Howell, R. Siegel, M. Pinar Menguc. Thermal radiation heat transfer. CRC press, New York, 2010.
20 P.Coss, A. Moses, and Y. C. Chang, Microwave regeneration of activated carbon used for removal of solvents from vented air, J. Air & Waste Management Association 50(4) (2000) 529-535.
21 S. W. Churchill, H. H. S. Chu, Correlating equations for laminar and turbulent free convection from a vertical plate, Int. J. Heat Mass Transfer, 18(11) (1975) 1323-1329.
22 G. F. C. Rogers, Y. R. Mayhew, Engineering Thermodynamics, Work and Heat Transfer, Longman, New York, 1992.
23 I. I. El-Sharkawy, K. Kuwahara, B. B. Saha, S. Koyama, K. C. Ng, Experimental investigation of activated carbon fibers/ethanol pairs for adsorption cooling system application, Applied Thermal Engineering, 26(8) (2006) 859-865.
24 I. S. Glaznev, Y. I. Aristov, The effect of cycle boundary conditions and adsorbent grain size on the water sorption dynamics in adsorption chillers, Int. J. Heat Mass Transfer, 53(9) (2010) 1893-1898.
25 E. Gluekauf, Theory of chromatography, part 10. Formula for diffusion into spheres and their application to chromatography, Trans. Faraday Soc. 51 (1955) 1540-1551.
26 A. Raymond, S. Garimella, Intraparticle mass transfer in adsorption heat pumps: limitations of the linear driving force approximation, J. Heat Transfer, 133(4) (2011) 042001-042001-13.
27 A. R. Rezk, R. K. Al-Dadah, Physical and operating conditions effects on silica gel/water adsorption chiller performance, Applied Energy, 89(1) (2012) 142-149.
28 H. T. Chua, K. C. Ng, W. Wang, C. Yap, X. L. Wang, Transient modeling of a two-bed silica gel–water adsorption chiller, Int. J. Heat Mass Transfer, 47(4) (2004) 659-669.
29 M. Ahamat, M. Tierney, Calorimeteric Assessment of Rates of Desorption, Proc., Innovative Materials for Processes in Energy Systems (IMPRES), Fukouka, Japan, (2013) 335-338.

369

370

**Figure Captions**

**Figure 1 Basic adsorption heat pump (a) layout (b) idealised thermodynamic cycle shown as Clapeyron Diagram. (1) Containment (2) adsorbent (between fins) (3) fin (4) tube-in-tube heat exchanger (5) base, sealing heat exchanger to adsorbent (6) three way valve (7) refrigerant vapour from evaporator (8) refrigerant vapour to condenser**

**Figure 2 Calorimeter (a) line drawing (b) photograph of essential items of interest. Items (1) heat exchanger (2) vessel lid (3) essential items of interest (4) thermoelectric module (TEM) (5) thermocouple locations (6) fin (7) fin gap - ACC filled (8) vessel casing (9) evaporator (10) water bath (V1, V2) valves (p) pressure gauge (Edwards model D 35726000) .**

**Figure 3 Finned sample partly filled with squares of activated carbon cloth. Only gaps 1, 4 and 6 are filled. Two squares are shown in the foreground.**

**Figure 4: Showing correction of raw heat flow. The vertical dotted line shows the start of the experiment. The set point temperature = 313 K**

**Figure 5 Temperature spikes within the ACC. Vapour pressure was raised from 0 to 19 mbar and the fin base was held at a constant temperature of 313 K**

**Fig. 6 Heat transfer following jump in vapour pressure (a) confirming exponential trends (b) Arrhenius plot of rate coefficients. Vapour pressure is 19 mbar**

**Fig. 7 Equilibrium loading. Temperatures were in the range from 313 K to 358 K and pressures in the range from 12 mbar to 35 mbar.**

**Figure 8. Outcome of a step change in temperature, or LTJ (a) measured and predicted heat transfer (b) ACC and base temperatures. Vapour pressure = 13 to 16 mbar. Symbols are $Q_a$, total heat measurement, $Q_l$ heat loss, $Q_x$ sensible heat, $T_b$ temperature of base**

**Figure 9 Fitting of heat rejection for (a) row 2 in Table 3 (b) row 4 in Table 3. Heat rejection $Q^{(a-l)}$ and $Q^{(a-lx)}$ are fitted. The fits are shown as dotted lines.**

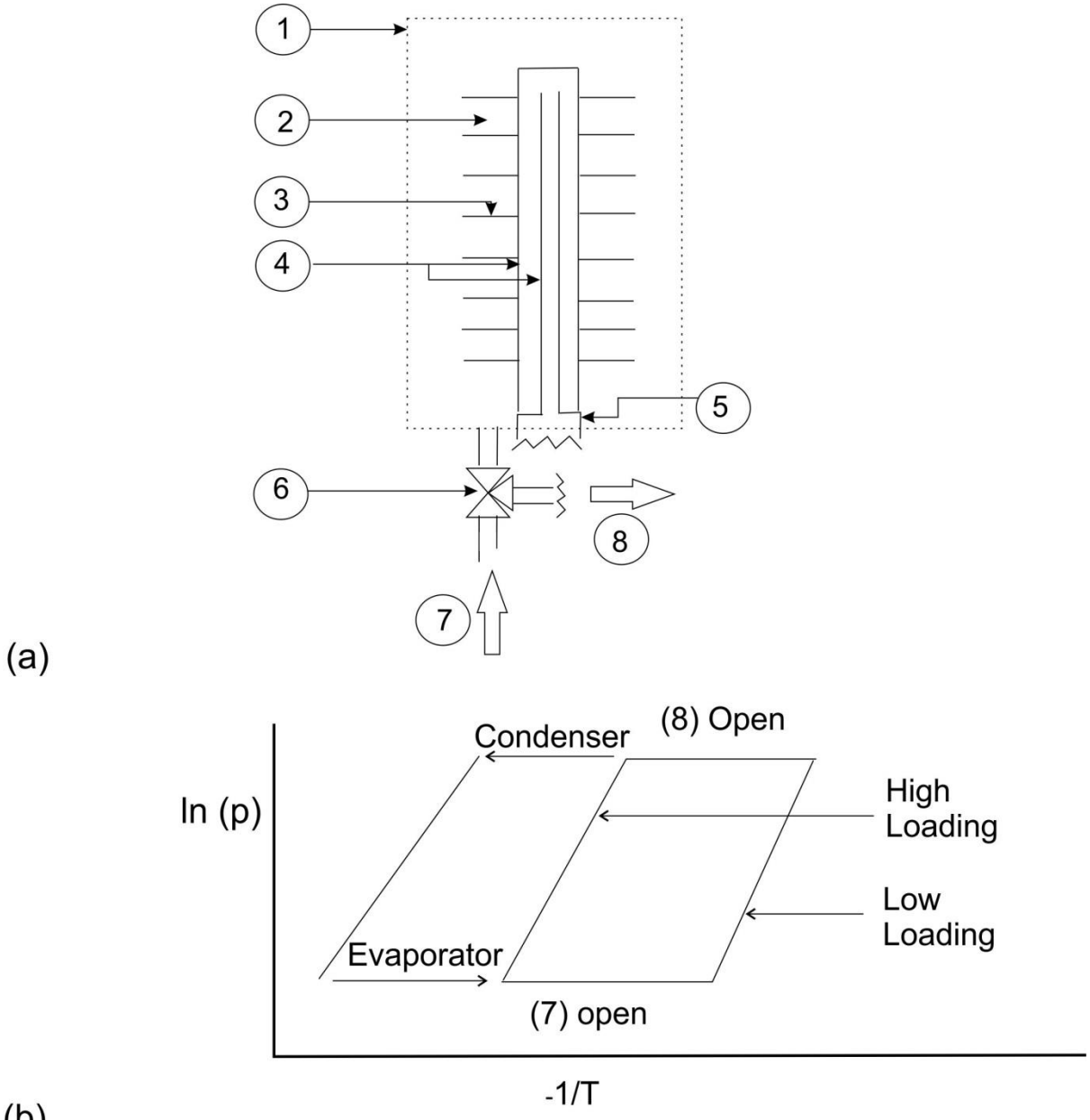


**Figure 1 Basic adsorption heat pump (a) layout (b) idealised thermodynamic cycle shown as Clapeyron diagram. (1) Containment (2) adsorbent (between fins) (3) fin (4) tube-in-tube heat exchanger (5) base, sealing heat exchanger to adsorbent (6) three way valve (7) refrigerant vapour from evaporator (8) refrigerant vapour to condenser.**

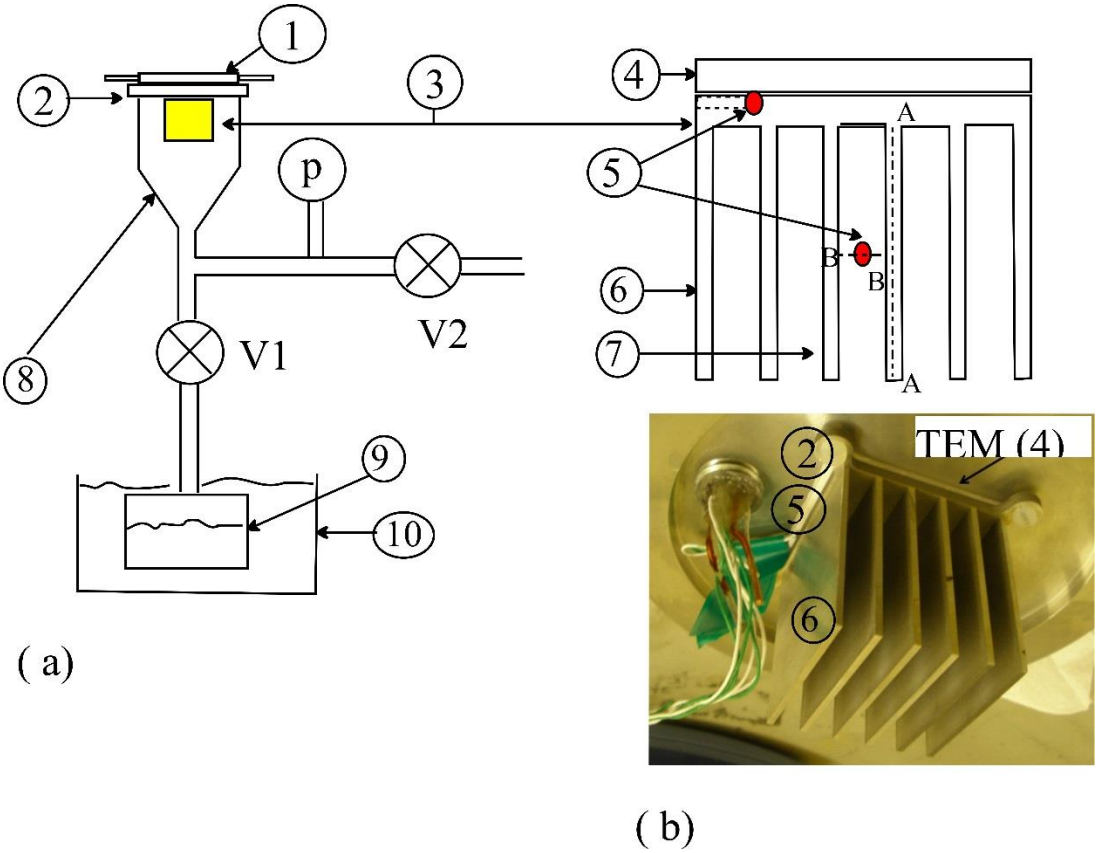


415

416

417 **Figure 2 Equipment (a) line drawing (b) photograph of essential items of interest. Items (1)**
418 **cooling apparatus (2) vessel lid (3) essential items of interest (4) thermoelectric module (TEM) (5)**
419 **thermocouple locations (6) fin (7) fin gap - ACC filled (8) vessel casing (9) evaporator (10) water**
420 **bath (V1, V2) valves (p) pressure gauge (Edwards model D 35726000). Dashed lines A-A and B-B**
421 **are the subjects of analysis in section 3. Dashed lines A-A and B-B are the subjects of analysis in**
422 **section 3.**

423

424

425

426

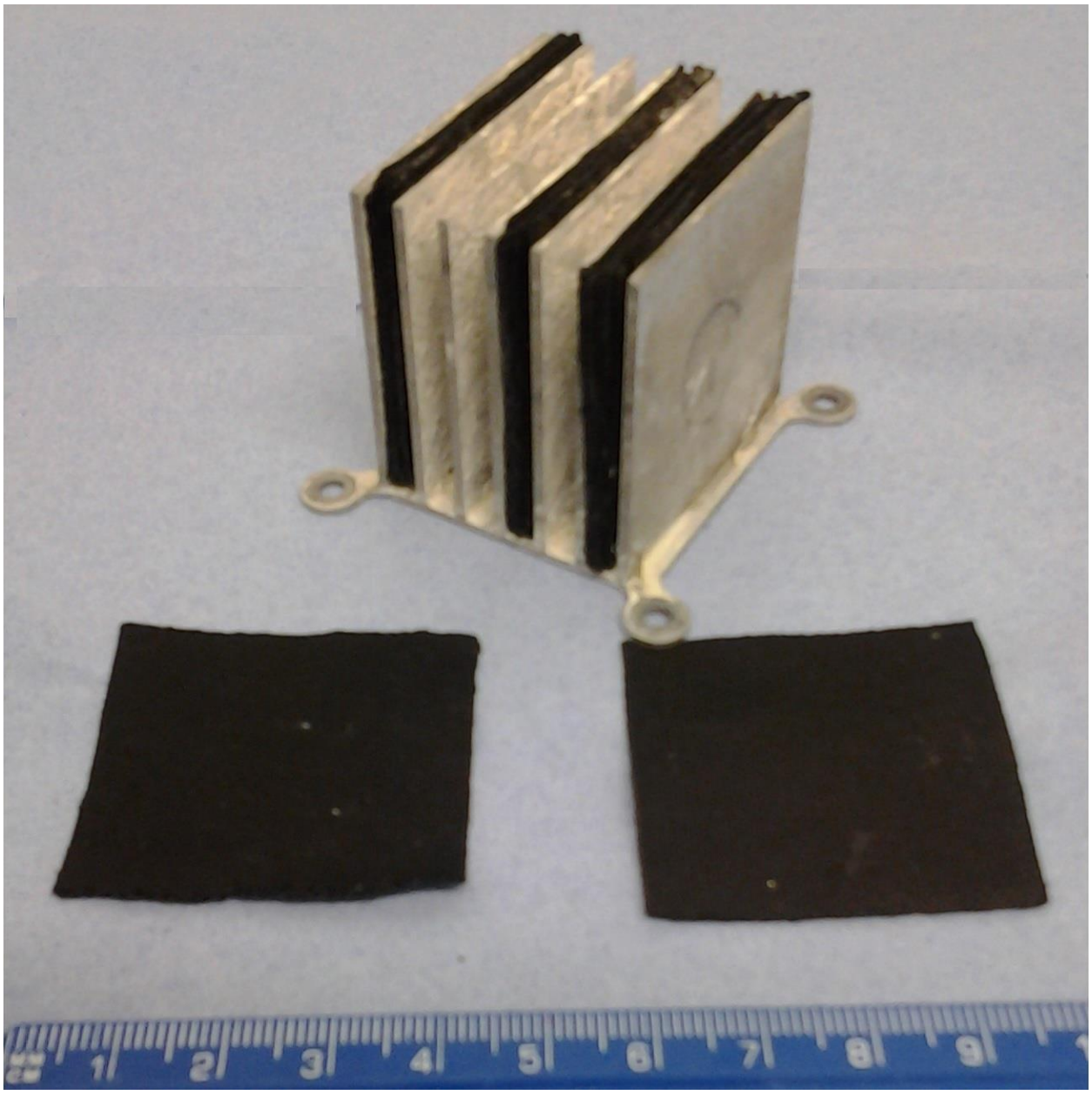

**Figure 3 Finned sample partly filled with squares of activated carbon cloth. Only gaps 1, 4 and 6 are filled. Two squares are shown in the foreground.**

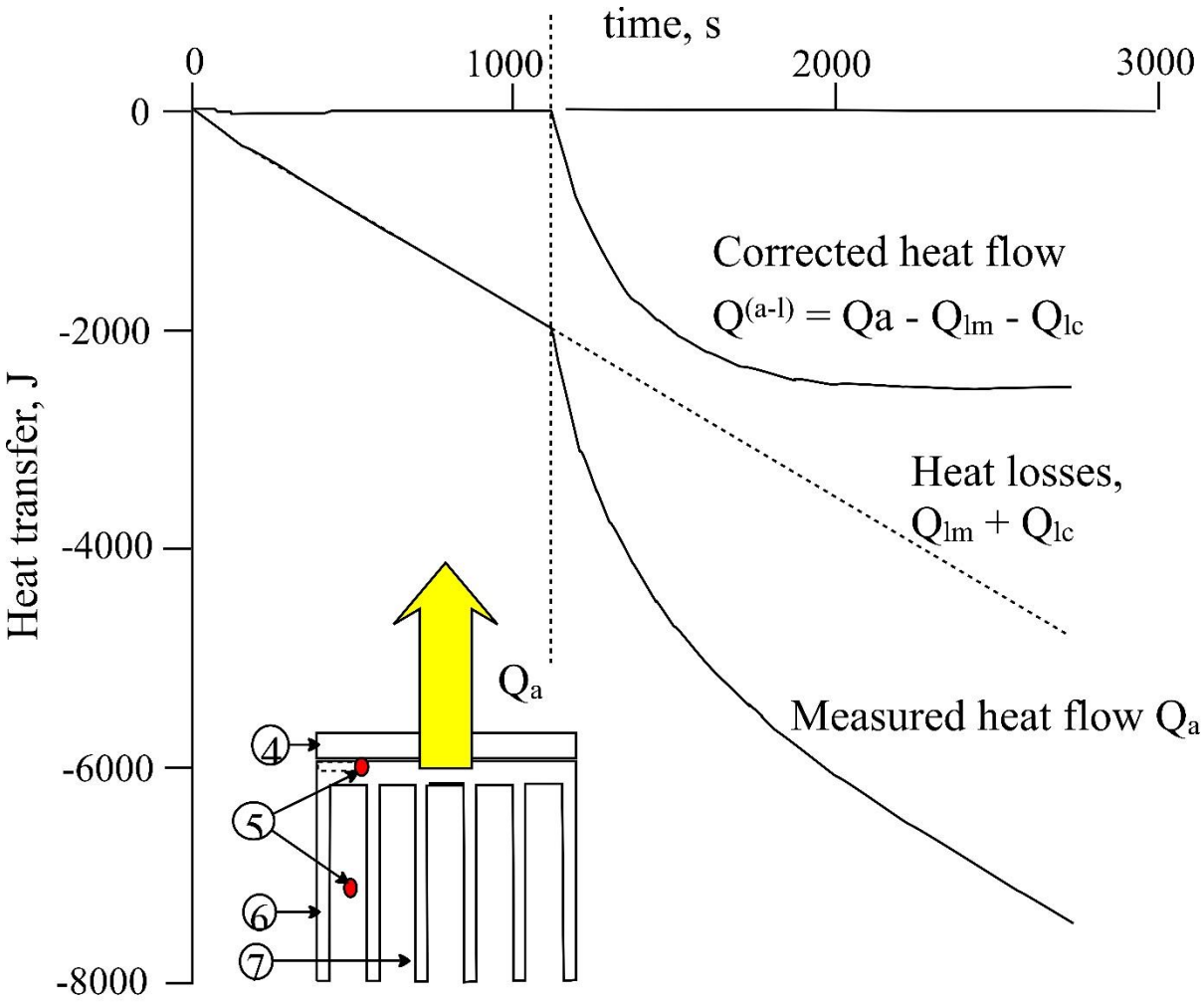


**Figure 4: Showing correction of raw heat flow. The vertical dotted line shows the start of the experiment. The set point temperature = 313 K**

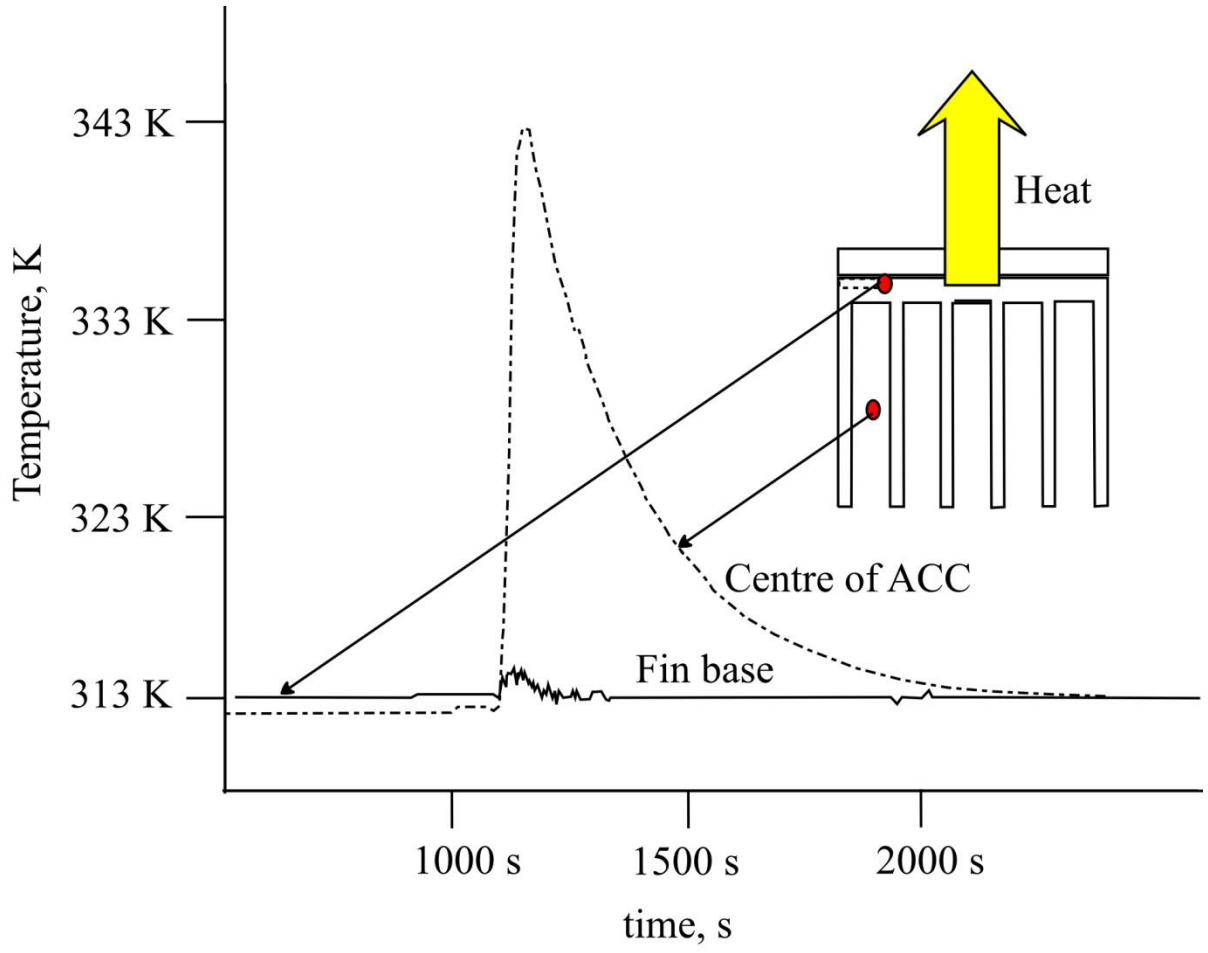


446

447

448 **Figure 5 Temperature spikes within the ACC. Vapour pressure was raised from 0 to 19 mbar and**
449 **the fin base was held at a constant temperature of 313 K**

450

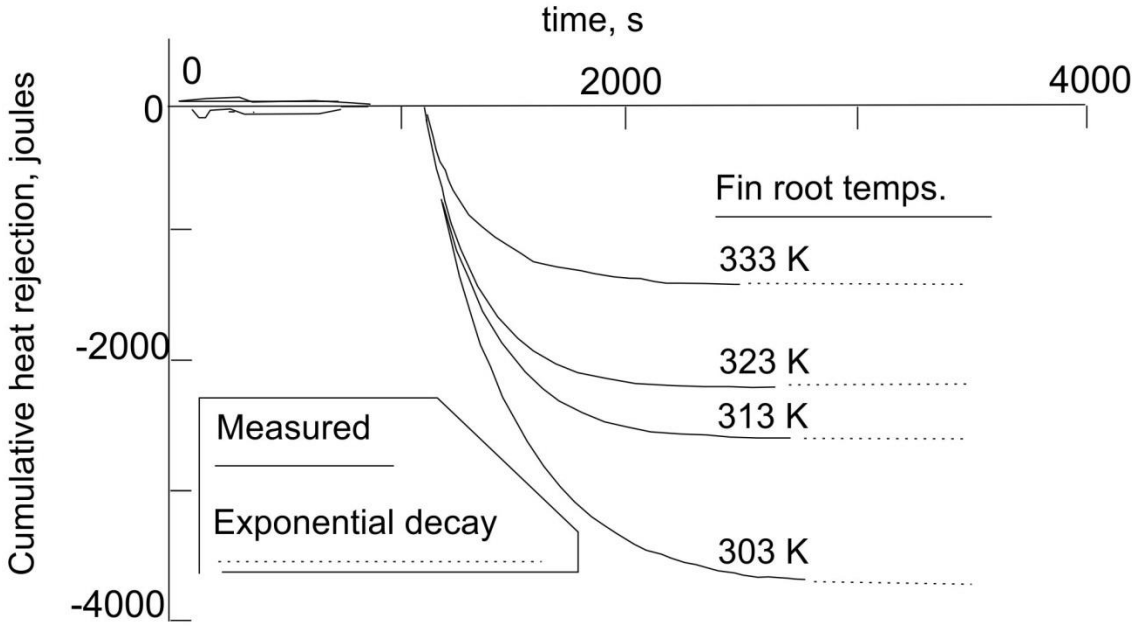


451

452 **Fig. 6 Heat transfer following jump in vapour pressure (a) confirming exponential trends (b)**
453 **Arrhenius plot of rate coefficients. Vapour pressure is 19 mbar**

454

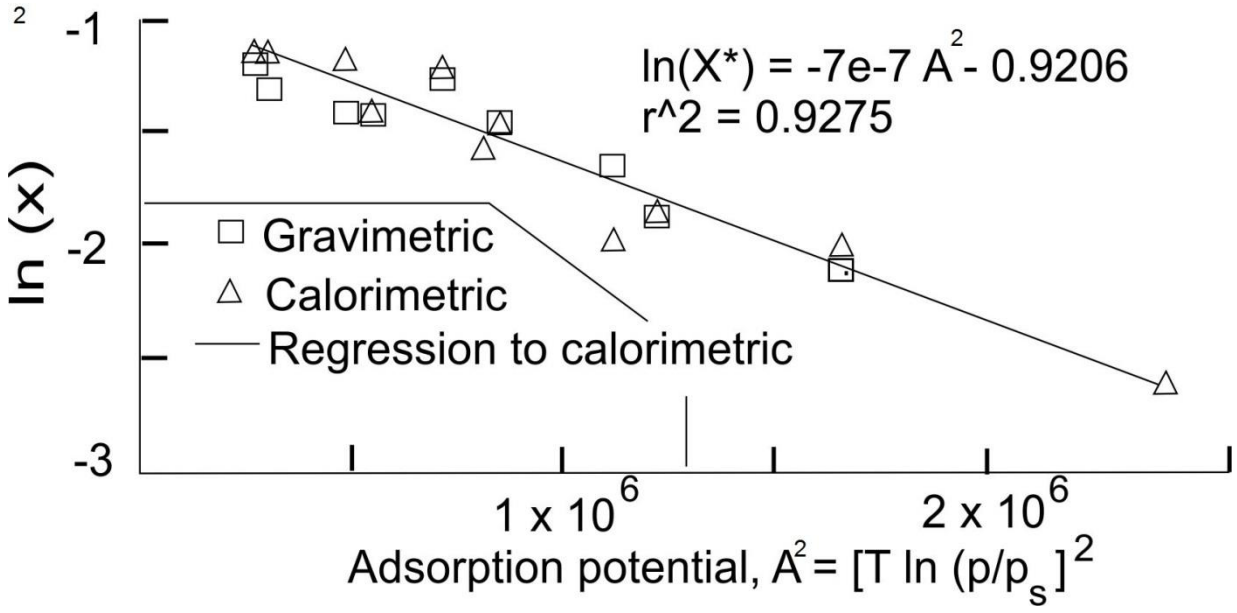


**Fig. 7 Equilibrium loading. Temperatures were in the range from 313 K to 358 K and pressures in the range from 12 mbar to 35 mbar**

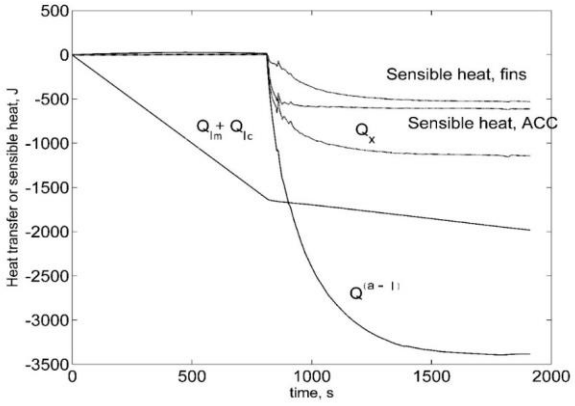


**(a)**

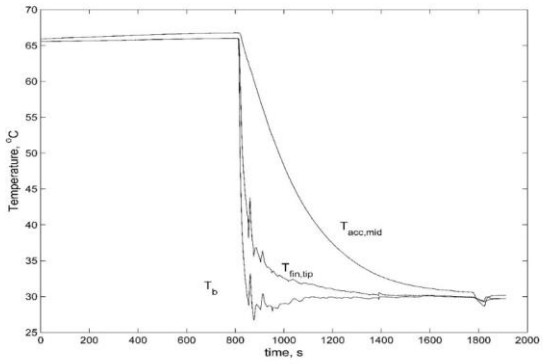


**(b)**

**Figure 8. Outcome of a step change in temperature, or LTJ (a) measured and predicted heat transfer (b) ACC and base temperatures. Vapour pressure = 13 to 16 mbar. Symbols are $Q^{(a-l)}$, coorected heat measurement, $Q_{lm}$ , Qlc heat losses used in correction, $Q_x$ sensible heat, $T_b$ temperature of base**

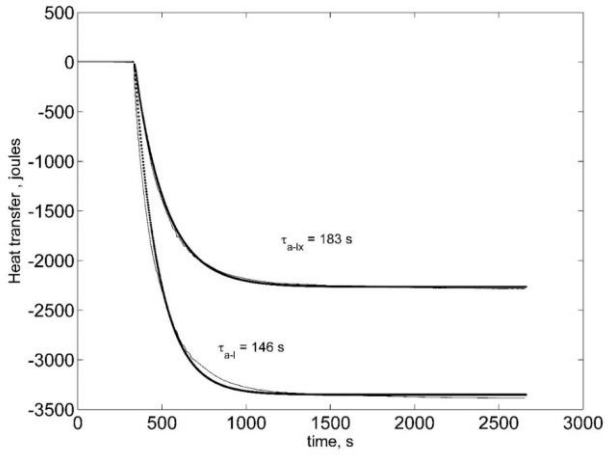


**(a)**

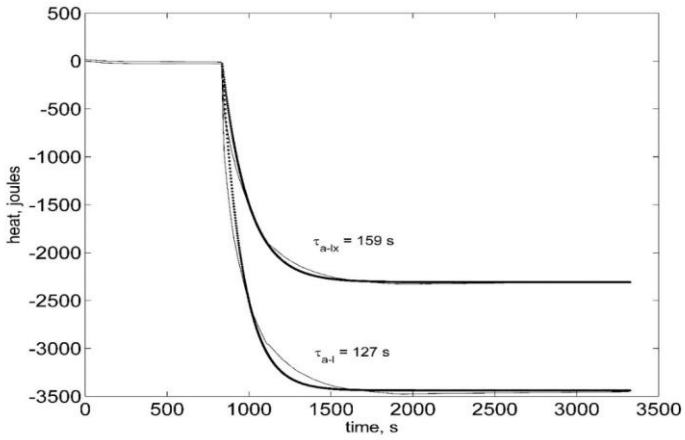


**(b)**

**Figure 9 Fitting of heat rejection for (a) row 1 in Table 3 (b) row 4 in Table 3. Heat rejection $Q^{(a\text{-}I)}$ and $Q^{(a\text{-}Ix)}$ are fitted. The fits are shown as dotted lines.**